https://doi.org/10.5194/egusphere-2026-5623
Preprint. Discussion started: 12 November 2026
© Author(s) 2026. CC BY 4.0 License.

VADERS v1.0: A Mechanistic Model for Vertical Atmospheric Dispersion of Biological Contaminants with Deposition, Resuspension, and Surface Inactivation

Michael S. Liboriussen[1,2] and Jesper S. Hansen[1]

[1]Department of Science and Environment, Roskilde University, Roskilde, Denmark
[2]Centre for Biosecurity and Biopreparedness, Statens Serum Institut, Copenhagen, Denmark

Correspondence: Michael S. Liboriussen (mskyttep@ruc.dk)

Abstract. A fundamental understanding of the processes governing atmospheric dispersion of contaminants is essential for optimizing the emergency response following a biological incident. We present a mechanistic, vertically resolved atmospheric dispersion model that couples advection and diffusion in the atmosphere with surface deposition, resuspension and decay due to inactivation through a flux-exchange lower boundary. Air-clearance time is compared for two analytically solved reference cases, namely (i) perfect contaminant deposition and (ii) zero contaminant deposition. The model is applied to scenarios with constant turbulent diffusivity, a linear parameterization of turbulent diffusivity, and time-dependent resuspension, and compared to the reference cases. These scenarios are studied numerically. A non-monotonic dependence of the air-clearance time on the ratio of resuspension rate to deposition velocity is observed. We refer to the parameter region in which the air-clearance time exceeds that of reference case (ii) as the overshoot regime. This behaviour is associated with a slowly evolving air-surface exchange state with airborne contaminant. This regime is observed both for the scenarios assuming constant turbulent diffusivity and the linear parametrization of the turbulent diffusivity. The time-dependent resuspension is a logistic decay function which can be used to emulate scenarios with time intervals of high and low traffic. The model provides a simplified framework for investigating atmospheric persistence and air-surface exchange processes and may serve as a building block for more comprehensive atmospheric dispersion models.

1 Introduction

The decontamination response following the 2001 anthrax letters incident in the U.S implied that some facilities could not be reopened for more than 2 years. For a larger-scale incident, the work with decontamination would be even more extensive Franco and Bouri (2010). It is therefore important to develop predictive tools that support authorities in decision-making during such events.

Modeling passive dispersion of particles in the atmosphere with surface deposition and resuspension has been done in a number of studies, see the review by Sehmel (1980a) for some of the early work. Henry et al. (2023) define resuspension as the process where particles re-entrain in to the atmosphere after deposition due to weather or mechanically inducement. In the case of surface contamination of a biological contaminant with high persistency after deposition, it cannot be neglected that

https://doi.org/10.5194/egusphere-2026-5623
Preprint. Discussion started: 12 November 2026
© Author(s) 2026. CC BY 4.0 License.

resuspension can cause hazardous exposure by inhalation for long-term periods (days to weeks) Layshock et al. (2012). In this case, emergency responders must include counter actions in their decision process such as evacuation and decontamination.

The aim of this work is to present a mechanistic model that includes advection, diffusion, deposition, resuspension, and surface inactivation processes that affect the spatio-temporal concentration of a biological contaminant in a column of air. Deposition, resuspension and decay due to inactivation of material are modeled through the lower boundary of the system. The model enables estimation of an air-clearance time, defined as the time at which the airborne contaminant mass decreases below a specified threshold value. The primary purpose of the model is to provide a mechanistic understanding of the interactions between atmospheric transport, deposition, resuspension, and surface inactivation and to quantify their influence on airborne persistence. We envision the framework as a building block for more comprehensive atmospheric dispersion models that may additionally include infective dynamics, flow around buildings, and other environmental processes.

2 Model Description

Fig. 1 conceptualizes the model. The model is a mechanistic description of the vertical processes governing atmospheric dispersion. It is not intended to model horizontal concentration gradients, building wakes, urban-canyon flow structures, or other three-dimensional flow phenomena. Instead, the model is designed to investigate the fundamental mechanisms governing vertical transport and air-surface exchange processes. Airborne biological contaminants, denoted A, undergo advective and diffusive transport due to gravitational settling and turbulent mixing, respectively. When the contaminants come into contact with the surface they may adhere to the surface (deposition). We denote the deposited contaminant A_s. At the surface contaminants can decay to an inert compound, B, or the contaminants can detach from the surface and be resuspended in air. Let the concentration of A be denoted a, with unit mass per length, and the mass of deposited contaminant A_s be denoted a_s. Then the conservation laws in one dimension read

$$\frac{\partial a}{\partial t} = -\frac{\partial J_a}{\partial z} \qquad (0 < z < L) \tag{1}$$

$$\frac{da_s}{dt} = r_d - r_s - r_r \qquad (z = 0) \tag{2}$$

where J_a is the flux of a, r_d the deposition rate, r_s is the resuspension rate, and r_r the decay rate of A_s into the inert compound. L is the characteristic height of the system. Applying Fick's law the flux of a is simply

$$J_a = -K_z \frac{\partial a}{\partial z} - v_{\text{set}} a\,, \tag{3}$$

where K_z is the turbulent diffusivity Taylor (1922); Richardson (1926); Sutton (1953), and v_{set} is the settling velocity of the contaminant due to gravitational pull. In general K_z and v_{set} are functions of position and time, i.e., $K_z = K_z(z,t)$ and $v_{\text{set}} = v_{\text{set}}(z,t)$. The rates for the deposited contaminant are given by

$$r_d = v_{\text{dep}} a,\ r_s = \Lambda_{\text{res}} a_s, \text{ and } r_r = \alpha a_s\ , \tag{4}$$

where v_{dep} is the deposition velocity, Λ_{res} the resuspension rate coefficient, and α is the decay rate coefficient. We have used the symbolism found in the literature Slinn (1976); Calder (1961); Nicholson (1988); Sehmel (1980b). The decay r_r is here a

https://doi.org/10.5194/egusphere-2026-5623
Preprint. Discussion started: 12 November 2026
© Author(s) 2026. CC BY 4.0 License.

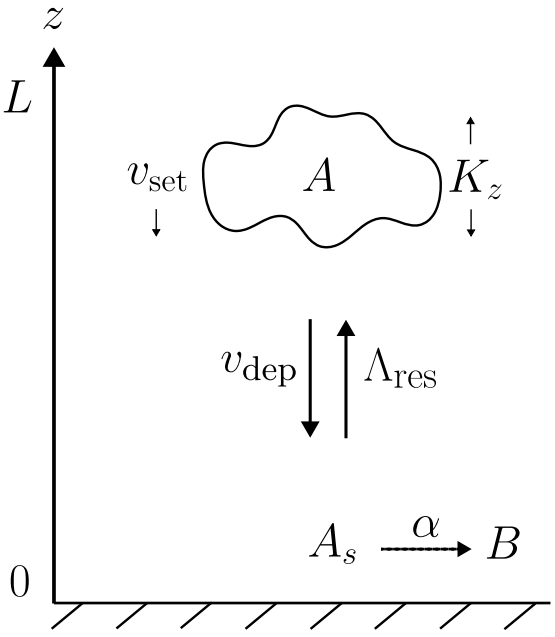


Figure 1. Illustration of the model mechanisms. The vertical dispersion of airborne contaminants, A, is governed by diffusion and advection. Contaminants can be deposited to the surface, A_s, and re-suspended into the air. Deposited contaminants may be removed by a given rate using active decontamination efforts or by simple decay giving rise to an inert compound, B. Rate constants are explained in the text, and L is the system characteristic height.

simple linear decay, however, r_r can take any functional form depending on the underlying bio-chemical processes and may also include effects of human infection.

We now introduce the following dimensionless quantities: $\tilde{a} = a/a_0$, $\tilde{a}_s = a_s/(a_0 \Delta z_s)$, $\tilde{z} = z/L$, and $\tau = (v_{\text{set}}/L)t$, where a_0 is a concentration value used for scaling and Δz_s is the thickness of the near-surface boundary layer. Substitution into the flux and rates we obtain

$$\frac{\partial \tilde{a}}{\partial \tau} = \frac{\partial}{\partial \tilde{z}} \left(\frac{1}{Pe} \frac{\partial \tilde{a}}{\partial \tilde{z}} \right) + \frac{\partial \tilde{a}}{\partial \tilde{z}} \qquad (0 < \tilde{z} < 1) \tag{5}$$

$$\frac{d\tilde{a}_s}{d\tau} = v^*_{\text{dep}} \tilde{a}_{z=0} - (\Lambda^*_{\text{res}} + \alpha^*) \tilde{a}_s \qquad (\tilde{z} = 0) \tag{6}$$

https://doi.org/10.5194/egusphere-2026-5623
Preprint. Discussion started: 12 November 2026
© Author(s) 2026. CC BY 4.0 License.

where $Pe = v_{\text{set}}L/K_z$ is the Peclet number and

$$v^*_{\text{dep}} = \frac{v_{\text{dep}}L}{v_{\text{set}}\Delta z_s}\,,\ \Lambda^*_{\text{res}} = \frac{\Lambda_{\text{res}}L}{v_{\text{set}}}\,,\ \text{and}\ \alpha^* = \frac{\alpha L}{v_{\text{set}}}\,. \tag{7}$$

The boundary at $z = L$ (upper boundary) is always a homogeneous Dirichlet boundary, i.e., in terms of dimensionless units

$$\tilde{a}(1,\tau) = 0\,. \tag{8}$$

This boundary condition models the removal of the biological contaminant by free flow above the boundary layer, where the contaminant concentration is zero. In the following we investigate the model predictions for the contaminant concentration in air and surface under different conditions at the lower boundary $z = 0$. To ease the reading we will, unless otherwise stated, omit the tilde notation for dimensionless quantities as well as replace τ with t.

2.1 Solutions to reference cases

In this section we solve the model for two limiting cases: (i) perfect deposition and (ii) zero deposition For both cases we let the Peclet number be constant, that is, Eq. (5) reads

$$\frac{\partial a}{\partial t} = \frac{1}{Pe}\frac{\partial^2 a}{\partial z^2} + \frac{\partial a}{\partial z}\,. \tag{9}$$

These two limiting cases serve as reference cases for the more general scenarios investigated in the next section. Analytical solutions to these linear problems are well-known see e.g. Refs. Farlow (1993) and Glinowiecka-Cox (2022), but for completeness we briefly outline the treatment and the results. A detailed derivation of case (ii) can be found in appendix A.

2.1.1 Case (i)

Here the agent concentration at $z = 0$ is zero due to the perfect deposition, thus, we have a homogeneous Dirichlet boundary

$$a(z,t) = 0 \qquad (z \to 0). \tag{10}$$

This case entails a drainage of A at both system boundaries. Importantly, the dynamics of a decouples a_s, i.e., we may seek the solution for a only using Eq. (9). The Dirichlet problem has the solution

$$a(z,t) = \phi(z,t)\sum_{n=1}^{\infty} A_n \sin(k_n z)\, e^{-\frac{k_n^2}{Pe}t}\,, \tag{11}$$

where $k_n \in \mathbb{R}$ is the wave vector, $k_n = n\pi, n \in \mathbb{N}_+$, and the Fourier coefficients are given by the initial distribution of the agents $a(z,0)$

$$A_n = 2\int_0^1 e^{\frac{Pe}{2}z} a(z,0)\sin(k_n z)\,\mathrm{d}z. \tag{12}$$

The pre-factor function ϕ depends on the Peclet number

$$\phi(z,t) = e^{-Pe\left(\frac{z}{2}+\frac{t}{4}\right)}\,. \tag{13}$$

https://doi.org/10.5194/egusphere-2026-5623
Preprint. Discussion started: 12 November 2026
© Author(s) 2026. CC BY 4.0 License.

It can be seen that $a \to 0$ as $t \to \infty$ for all $z \in [0;1]$, thus, the steady-state solution is the trivial solution as expected with the Dirichlet boundaries.

2.1.2 Case (ii)

In the case of zero deposition we obtain a no-flux boundary (zero deposition)

$$\frac{\partial a(z,t)}{\partial z} + Pe\, a(z,t) = 0 \qquad (z \to 0) \tag{14}$$

This is also known as a Robin boundary. The solution is on the form

$$a(z,t) = \phi(z,t)\left(Y_0(z,t) - Y_1(z,t)\right), \tag{15}$$

where

$$Y_0 = \chi_0(z,t) + \sum_{n=1}^{\infty} A_n \cos(\kappa_n z)\, e^{-\frac{\kappa_n^2}{Pe}t} \tag{16}$$

and

$$Y_1 = \chi_1(z,t) + \frac{Pe}{2}\sum_{n=1}^{\infty} \frac{A_n}{\kappa_n} \sin(\kappa_n z)\, e^{-\frac{\kappa_n^2}{Pe}t}. \tag{17}$$

The wave vector $\kappa_n \in \mathbb{R}$ is given by the non-linear relation $\tan(\kappa_n) = 2\kappa_n/Pe$; see appendix A for details. In the situation where $Pe \geq 2$ the relation allows for an additional fundamental solution and the functions χ_0 and χ_1 are defined as

$$\chi_0(z,t) = \begin{cases} 0, & \text{if } Pe < 2 \\ A_0, & \text{if } Pe = 2 \\ A_{\kappa_0} \cosh(\kappa_0 z)\, e^{\frac{\kappa_0^2}{Pe}t}, & \text{if } Pe > 2, \end{cases} \tag{18}$$

and

$$\chi_1(z,t) = \begin{cases} 0, & \text{if } Pe < 2 \\ A_0 z, & \text{if } Pe = 2 \\ \frac{Pe}{2}\frac{A_{\kappa_0}}{\kappa_0} \sinh(\kappa_0 z)\, e^{\frac{\kappa_0^2}{Pe}t}, & \text{if } Pe > 2\,. \end{cases} \tag{19}$$

The Fourier coefficients for $n \in \mathbb{N}_+$ are given by

$$A_n = \frac{\int_0^1 \cos(\kappa_n z) - \frac{Pe}{2\kappa_n}\sin(\kappa_n z)\, e^{\frac{Pe}{2}z} a(z,0)\,\mathrm{d}z}{\int_0^1 \left(\cos(\kappa_n z) - \frac{Pe}{2\kappa_n}\sin(\kappa_n z)\right)^2 \mathrm{d}z}. \tag{20}$$

For $Pe > 2$ we also have

$$A_{\kappa_0} = \frac{\int_0^1 \cosh(\kappa_0 z) - \frac{Pe}{2\kappa_0}\sinh(\kappa_0 z)\, e^{\frac{Pe}{2}z} a(z,0)\,\mathrm{d}z}{\int_0^1 \left(\cosh(\kappa_0 z) - \frac{Pe}{2\kappa_0}\sinh(\kappa_0 z)\right)^2 \mathrm{d}z}. \tag{21}$$

https://doi.org/10.5194/egusphere-2026-5623
Preprint. Discussion started: 12 November 2026
© Author(s) 2026. CC BY 4.0 License.

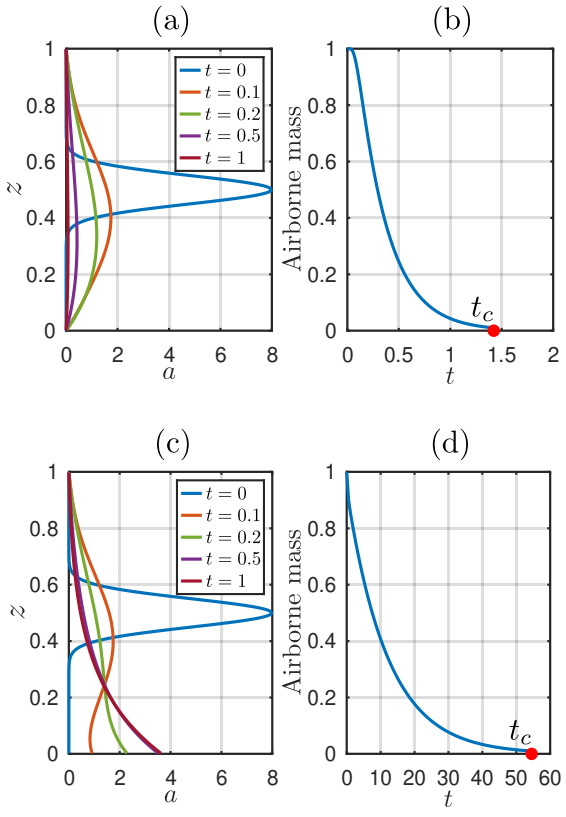


Figure 2. Concentration profiles for different times and airborne mass with respect to time; dimensionless time $t = 1$ corresponds to approximately 9 hours. (a) and (b): Case (i) - perfect deposition. (c) and (d): Case (ii) - zero deposition. In both cases the Peclet number is 4. The initial condition is given by Eq. (25), and t_c is the air-clearance time see Eq. (26).

For the case where $Pe = 2$, A_0 is calculated from Eq. (20) when $\kappa_n \to 0$. Again, one can see that the steady state solution, $a = 0$, is the trivial zero solution. Fig. 2 shows an example of the concentration profiles for case (i) and case (ii) as function of time for Pe=4 with a Gaussian distribution as initial conditons, see Eq. (25). One clearly sees that the contaminant drains from the system much quicker for case (i) compared to case (ii); which is expected.

2.2 Relaxation time

Case (i): From distribution of the prefactor ϕ, Eq. (13), into the Fourier series in Eq. (11) one can see that each term in the series has a characteristic relaxation time $t_n = 4Pe/\left(Pe^2 + 4k_n^2\right)$. This means that each Fourier mode feature a non-monotonic

https://doi.org/10.5194/egusphere-2026-5623
Preprint. Discussion started: 12 November 2026
© Author(s) 2026. CC BY 4.0 License.

relaxation with respect to the Peclet number. We define two regimes

small Pe: $t_n \propto Pe$

large Pe: $t_n \propto 1/Pe$.

That is, for small Peclet numbers (diffusion dominated) the decay rate for a given mode decreases for increasing Pe, whereas for large Peclet numbers (advection dominated) the decay rate increases with increasing Pe.

Case (ii): When $Pe < 2$ we have the same relation for a given Fourier mode as in the first regime for small Pe in case (i). When $Pe > 2$ in case (ii) the additional wave vector, κ_0, dominates the relaxation time of the system, implying a much higher value than for the modes with $n > 0$ since

$$t_0 = \frac{1}{\frac{Pe}{4} - \frac{\kappa_0^2}{Pe}} \quad \text{and} \tag{22}$$

$$t_n = \frac{1}{\frac{Pe}{4} + \frac{\kappa_n^2}{Pe}}. \tag{23}$$

For large Pe in case (ii), we have that $t_0 \gg t_n$ with an exponential increasing relaxation for the additional wave vector

large Pe: $t_0 \propto \frac{1}{Pe} e^{Pe}$,

see Appendix A, section A4 for a detailed derivation.

3 Example Applications

For general scenarios, we define the lower boundary $z \to 0$ as a Robin-like boundary with flux exchange to and from the surface, as presented in Slinn (1976),

$$\frac{\partial a(z,t)}{\partial z} + Pe\, a(z,t) = v^*_{\text{dep}} a(z,t) - \Lambda^*_{\text{res}} a_s(t) \qquad (z \to 0). \tag{24}$$

Using this boundary and the initial condition in Eq. (25) we will study different scenarios as predicted by the model from numerical solutions using a standard finite volume scheme, see appendix B for model verification. To our knowledge, no suitable validation data are currently available for the specific application considered here.

3.1 Model setup

In this section we present the model parameters, K_z, L, v_{set} and v_{dep} with dimensions. The parameter values used throughout the study are summarized in Table 1. In all scenarios except the case with linear parametrization of K_z, we use an effective constant value of $K_z = 0.075\,\text{m}^2\,\text{s}^{-1}$ which implies $Pe = 4$ with $L = 100\,\text{m}$. The settling velocity is set to $v_{\text{set}} = 3 \times 10^{-3}\,\text{m}\,\text{s}^{-1}$ based on Stokes' law for particles with a diameter of $10\,\mu\text{m}$, Salem and Katz (2016). We choose $v_{\text{dep}} = 5 \times 10^{-4}\,\text{m}\,\text{s}^{-1}$ (a low estimate for $10\,\mu\text{m}$ particles, see for example Sehmel (1980b) and Giardina and Buffa (2018)). When investigating the dependence on $\Lambda^*_{\text{res}}/v^*_{\text{dep}}$ the resuspension rate is varied over the range $\Lambda_{\text{res}} = 1.25 \times 10^{-7}\,\text{s}^{-1}$ to $6.25 \times 10^{-1}\,\text{s}^{-1}$. The range was chosen to

https://doi.org/10.5194/egusphere-2026-5623
Preprint. Discussion started: 12 November 2026
© Author(s) 2026. CC BY 4.0 License.

Table 1. Parameter ranges used in this study; see text for references

K_z [$\mathrm{m^2\,s^{-1}}$]	v_{set} [$\mathrm{m\,s^{-1}}$]	v_{dep} [$\mathrm{m\,s^{-1}}$]	Λ_{res} [$\mathrm{s^{-1}}$]	α [$\mathrm{s^{-1}}$]
0.075 – 1	3×10^{-3}	5×10^{-4}	1.25×10^{-7} – 6.25×10^{-1}	0 – 5×10^{-3}

ensure that the corresponding values of $\Lambda^*_{\mathrm{res}}/v^*_{\mathrm{dep}}$ encompass the full spectrum of air-clearance time behaviour bounded by the two reference cases for $\alpha = 0$. The initial condition is set to be a Gaussian distribution, in dimensionless form

$$a(z,0) = \frac{1}{\sqrt{2\pi}\sigma} e^{\frac{-(z-0.5)^2}{2\sigma^2}}, \tag{25}$$

where $\sigma = 0.05$. Note that we have chosen an initial condition where the total dimensionless mass is 1.

3.2 Air-clearance time

The air-clearance time, t_c, is introduced as a diagnostic metric for comparing model behaviour across scenarios. It should not be interpreted as a risk metric or an operational decision threshold directly. Rather, it is used here as a measure of airborne persistence and is defined as the first time at which the airborne contaminant mass falls below a prescribed threshold value

$$\int_0^1 a(z,t_c)\,dz = C, \tag{26}$$

we choose $C = 0.01$ in this study corresponding to $1\,\%$ mass remaining. It is important to note that t_c only gives a time measure of air concentration and not surface concentration. If the surface concentration enters the definition, the values of t_c will be different by orders of magnitude depending on the specific scenario. For example, when $\alpha = 0$ the only drainage is through the upper boundary. Here the values of t_c will strongly depend on the size of the fraction of the resuspension rate and deposition velocity. For small fractions, deposited material re-enters the air at a slow rate after some time, giving very large values of t_c. The air-clearance time is used throughout this study because it provides a simple measure of airborne persistence and allows direct comparison with the reference cases. The relationship between t_c and Pe for cases (i) and (ii) is shown in Fig. 3. As expected, t_c increases with increasing Pe for both cases in the Peclet number interval studied here, and is relatively larger for case (ii). For case (i) this indicates that we are in the diffusion controlled regime. For case (ii), the increase in t_c begins to show the exponential relationship on Pe in this regime as predicted in section 2.2.

3.3 Scenarios with constant effective value for K_z

For comparison with the reference cases we choose constant effective values of K_z. Here we present two scenarios: One that models the dynamics with, and one without inactivation of contaminant deposited on the surface. The inactivation is modeled with a linear decay, and mimics the removal process by active decontamination or by simple decay of material. The air-clearance times t_c are shown in Fig. 4 (a) for these scenarios. The curves in Fig. 4 (a) show the relationship between t_c and the fraction $\Lambda^*_{\mathrm{res}}/v^*_{\mathrm{dep}}$ where $v_{\mathrm{dep}} = 5 \times 10^{-4}\,\mathrm{m\,s^{-1}}$ for $Pe = 4$. The blue curve is with no inactivation, $\alpha = 0$. This relation has

https://doi.org/10.5194/egusphere-2026-5623
Preprint. Discussion started: 12 November 2026
© Author(s) 2026. CC BY 4.0 License.

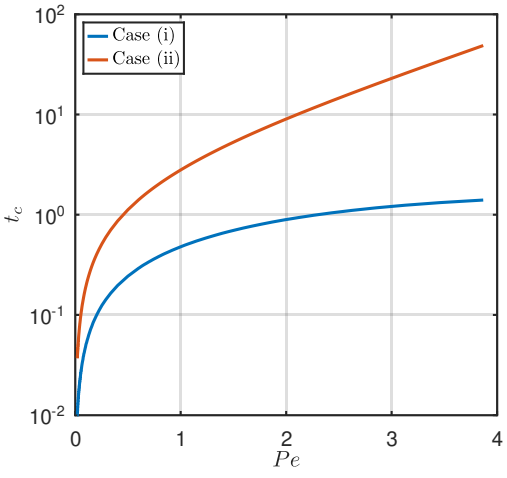


Figure 3. The relation between the air-clearance time and Pe for reference cases (i) and (ii). Notice the logarithmic scale on the second axis

also been studied for Peclet numbers in the same range as for the reference cases, and shows the same characteristics except for faster air-clearance times for decreasing Pe. A non-monotonic dependence of t_c on $\Lambda^*_{\text{res}}/v^*_{\text{dep}}$ is observed. We refer to the region in which t_c exceeds the values obtained from case (ii) as the overshoot regime. This overshoot is associated with a slowly evolving air-surface exchange state with a small flux of contaminant from the surface to the air, which is seen in Fig. 5 (c). The total flux exchange from the surface to the air near the lower boundary, is given by

$$J_{\text{surf}\to\text{air}}(t) = \Lambda^*_{\text{res}} a_s(t) - v^*_{\text{dep}} a(z,t) \qquad (z \to 0), \tag{27}$$

and is positive in positive z-direction. When the system reaches the slowly evolving air-surface exchange state ($t > 1$) there is a small rate of change of mass in the air. Consequently the air-clearance time metric becomes highly sensitive to the remaining airborne mass in this state. For solutions in which the airborne mass remains above the threshold value C, illustrated by the dashed line in Fig. 5(a), large values of t_c are obtained. For sufficiently large values of $\Lambda^*_{\text{res}}/v^*_{\text{dep}}$, less material deposits on the surface and the system does not reach a slowly evolving air-surface exchange state. In these cases there is a large flux of material out of the upper boundary and the system approaches t_c for case (ii) as mentioned before, see Fig. 5 (b). By adding a decay for deposited material, α, the overshoot decreases and vanishes for increasing α. This is due to the fact that less material

https://doi.org/10.5194/egusphere-2026-5623
Preprint. Discussion started: 12 November 2026
© Author(s) 2026. CC BY 4.0 License.

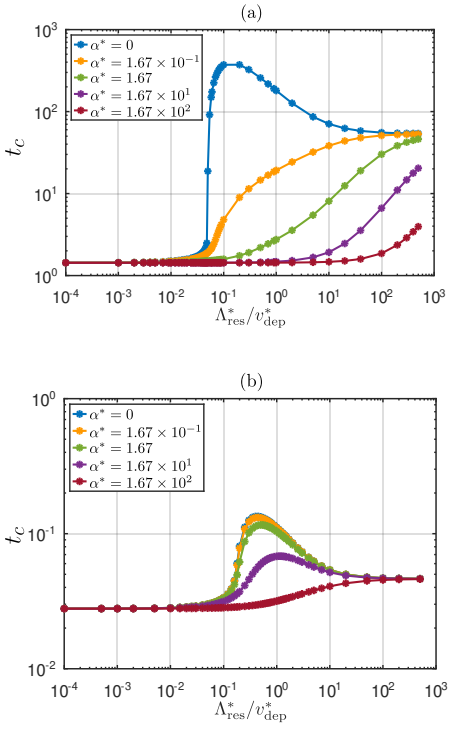


Figure 4. Relation between t_c and the fraction $\Lambda^*_{\mathrm{res}}/v^*_{\mathrm{dep}}$ where $v_{\mathrm{dep}} = 5 \times 10^{-4}\,\mathrm{m\,s^{-1}}$. (a): $Pe = 4$, (b): $Pe(z)$ given by Eq. (29) with $v_{\mathrm{set}} = 3 \times 10^{-3}\,\mathrm{m\,s^{-1}}$, $\kappa = 0.4$ and $u_* = 0.3\,\mathrm{m\,s^{-1}}$. Lines serve as a guide to the eye.

is available for resuspension which implies a faster air-clearance time. In general t_c decreases for increasing α for a given $\Lambda^*_{\mathrm{res}}/v^*_{\mathrm{dep}}$.

3.4 Linear model for K_z

Parametrization of the turbulent diffusivity, $K_z = K_z(z)$, depends on the atmospheric conditions. We have here chosen a linear model

$$K_z(z) = \kappa u_* z, \tag{28}$$

where κ and u_* is the von Karman's constant and friction velocity, respectively. This model is valid in a neutral atmosphere for flat terrain in the surface boundary layer Monin and Obukhov (1954); Stull (1988). Introducing a spatial dependency for K_z

https://doi.org/10.5194/egusphere-2026-5623
Preprint. Discussion started: 12 November 2026
© Author(s) 2026. CC BY 4.0 License.

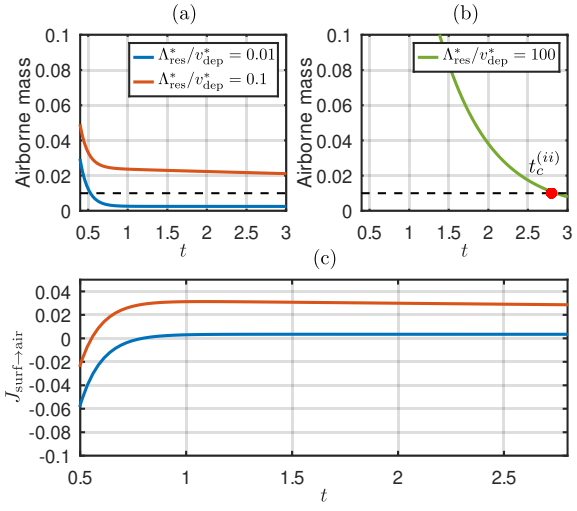


Figure 5. Illustration of the system dynamics with $Pe = 1$ and varying $\Lambda^*_{\rm res}$. (a) and (b) shows the airborne mass with respect to time where the dashed horizontal line illustrates the fraction of material which is left in the air with $C = 0.01$, and the red marker is the air-clearance time for case (ii). (c) illustrates the flux exchange of contaminant near the surface with respect to time given by Eq. (27), and is positive in positive z-direction.

implies a hyperbolic spatial dependency for the Peclet number

$$Pe(z) = \frac{v_{\rm set} L}{\kappa u_* z}. \tag{29}$$

Note that z in Eq. (29) has dimensions. At the lower boundary Pe is defined using the height of the near-surface boundary layer, $\Delta z_s = 0.4\,\mathrm{m}$. The friction velocity is estimated to $u_* = 0.3\,\mathrm{m\,s^{-1}}$ from the wind profile, Stull (1988),

$$u_* = \frac{u(z)\kappa}{\ln(z/z_0)}, \tag{30}$$

with a near surface ($z = 0.4\,\mathrm{m}$) wind velocity $u \approx 2.2\,\mathrm{m\,s^{-1}}$, a roughness length $z_0 = 0.02\,\mathrm{m}$ corresponding to a flat terrain, and the von Karman's constant $\kappa = 0.4$. Keeping $v_{\rm set}$ constant the discretization of the system gives the range of values of $K_z(z) \in [0.024; 12]$ for $0.4\,\mathrm{m} < z < 100\,\mathrm{m}$ which implies that $Pe(z) \in [0.025; 12.5]$. As the range of $Pe(z)$ spans 3 orders of magnitude, this affects the dynamics of the concentration profiles compared to cases with a constant value of K_z, see Fig. 6.

https://doi.org/10.5194/egusphere-2026-5623
Preprint. Discussion started: 12 November 2026
© Author(s) 2026. CC BY 4.0 License.

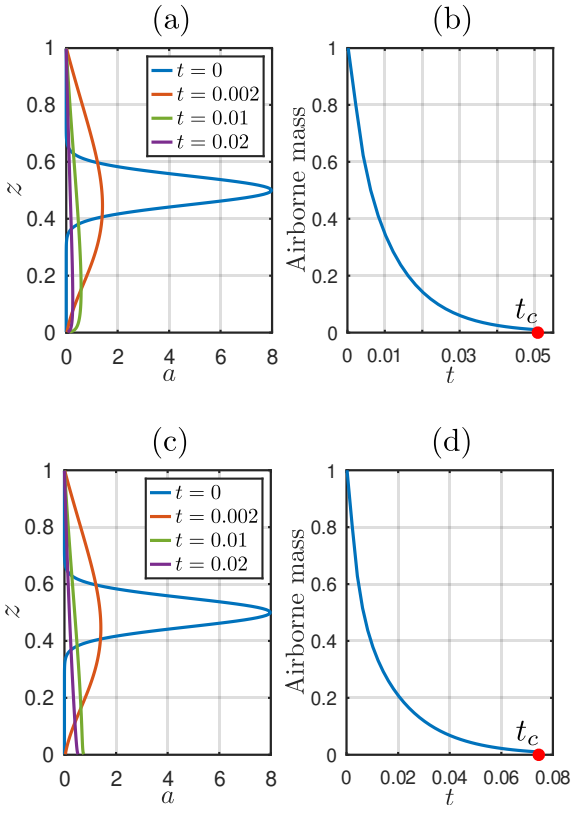


Figure 6. Concentration profiles for different (dimensionless) times and airborne mass with respect to time; $t = 1$ corresponds to approximately 9 hours. (a) and (b): $\Lambda^*_{\text{res}}/v^*_{\text{dep}} = 0.01$. (c) and (d): $\Lambda^*_{\text{res}}/v^*_{\text{dep}} = 1000$ - approximating zero deposition. Both cases use the linear model for $K_z(z)$ as in Eq. (28). The initial condition is given by Eq. (25).

Fig. 4 (b) shows the air-clearance times with respect to $\Lambda^*_{\text{res}}/v^*_{\text{dep}}$ for this scenario. The blue curve is almost merged with the orange curve where $\alpha = 1.67 \times 10^{-1}$ meaning there is no significant change in t_c. Note that this scenario also implies an overshoot in the air-clearance time that decreases and vanish for increasing α. In general the values of t_c are much lower than for the scenarios with constant K_z, which is caused by the range of values of $K_z(z)$. With physical dimensions the air-clearance times is approximately 30-40 minutes in the interval of $\Lambda^*_{\text{res}}/v^*_{\text{dep}}$ studied here.

3.5 Time-dependent resuspension rate

With a time-dependent resuspension rate it is possible to simulate scenarios with time-intervals of high and low traffic. In a real situation one could expect an undetected release of a biological contaminant which will not affect the daily traffic until the

https://doi.org/10.5194/egusphere-2026-5623
Preprint. Discussion started: 12 November 2026
© Author(s) 2026. CC BY 4.0 License.

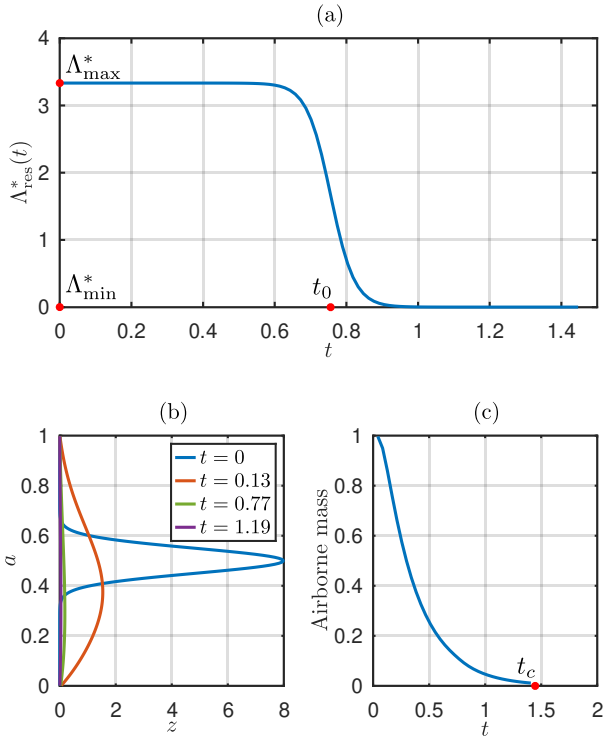


Figure 7. (a): Illustration of the scaled resuspension rate with related to τ, $\Lambda^*_{\mathrm{res}}(\tau)$, determined by a logistic decay function, see Eq. (31), with $r = 30$ and $t_0 = 0.76$. The physical values of the resuspension rate coefficients are $\Lambda_{\min} = 5 \times 10^{-8}\,\mathrm{s}^{-1}$ and $\Lambda_{\max} = 1 \times 10^{-4}\,\mathrm{s}^{-1}$. (b) and (c): Concentration profiles for different times and airborne mass with respect to time.

release is detected and the operational activities of the first responders are initiated. By choosing a logistic decay function we can model this scenario for given time-intervals

$$\Lambda^*_{\mathrm{res}}(t) = \Lambda^*_{\min} + \frac{\Lambda^*_{\max} - \Lambda^*_{\min}}{1 + e^{r(t-t_0)}}, \tag{31}$$

where $\Lambda_{\min} = 5 \times 10^{-8}\,\mathrm{s}^{-1}$ and $\Lambda_{\max} = 1 \times 10^{-4}\,\mathrm{s}^{-1}$ emulates the resuspension rates for low and high traffic, and r and t_0 are some rate constant and the inflection time respectively. Note that Λ^*, r, t and t_0 is non-dimensionsalized in Eq. (31). The value of $\Lambda_{\min}$ roughly estimates a low wind induced resuspension rate Sehmel (1980a), and $\Lambda_{\max}$ is arbitrarily chosen to estimate a vehicle induced resuspension rate. Fig. 7 (a) illustrates the logistic decay function model for $\Lambda^*_{\mathrm{res}}(\tau)$ with $r = 30$ and $t_0 = 0.76$. Fig. 7 (b) and (c) shows the concentration profiles for given values of time and airborne mass with respect to time, respectively. The value of $\Lambda^*_{\max}$ lies in the overshoot regime for $v_{\mathrm{dep}} = 5 \times 10^{-4}\,\mathrm{m\,s}^{-1}$, see Fig. 4 for $\Lambda^*_{\max}/v^*_{\mathrm{dep}} = 0.08$, which contributes to higher t_c-values depending on the value of the inflection time t_0. When t_0 exceeds the corresponding air-clearance time it is constant matching the ones for the given fraction of $\Lambda^*_{\mathrm{res}}/v^*_{\mathrm{dep}}$, see Fig. 8 for $Pe = 0.3$.

https://doi.org/10.5194/egusphere-2026-5623
Preprint. Discussion started: 12 November 2026
© Author(s) 2026. CC BY 4.0 License.

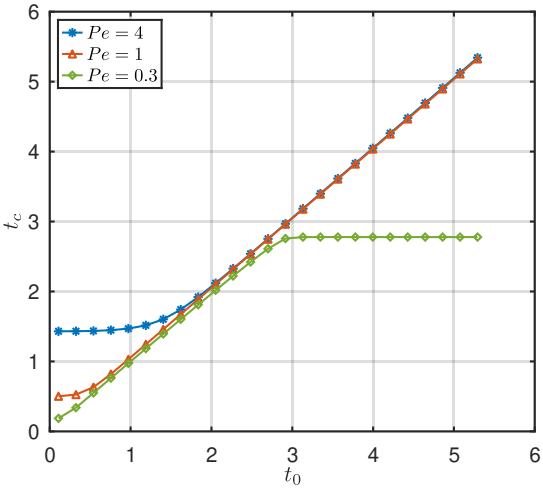


Figure 8. Relation of air-clearance time, t_c, and inflection time, t_0, for the model with $Pe = 0.3, 1, 4$ and $\alpha = 0$. Note that t_c and t_0 are dimensionless. Lines serve as a guide to the eye.

4 Conclusion

We presented a mechanistic model for investigating vertical atmospheric dispersion coupled with deposition, resuspension, and surface inactivation processes through a flux-exchange lower boundary. The framework is intended to provide insight into the interactions between atmospheric transport and air-surface exchange.

We apply the model to selected scenarios with a measure of how fast material is cleared from the air. Assuming a constant effective value of the turbulent diffusion, K_z, we found analytical solutions to the reference cases (i) and (ii), assuming perfect deposition and zero deposition, respectively. For case (i) the relaxation times of the system is proportional to the Peclet number for small Peclet numbers and inverse proportional to the Peclet number for large Peclet numbers. For Case (ii) we have the same relation as for case (i) for small Peclet numbers, and an exponential relationship for large Peclet numbers. These results indicates that the studied range of Peclet numbers is in the diffusion controlled regime for case (i). For case (ii) the large values in the range of Peclet numbers begin to show the exponential relationship.

https://doi.org/10.5194/egusphere-2026-5623
Preprint. Discussion started: 12 November 2026
© Author(s) 2026. CC BY 4.0 License.

The numerical solutions to the model in the scenarios where we allowed an exchange of material in the surface layer, we found regimes where the air-clearance time overshoots that of case (ii) for constant K_z. This overshoot decreases and vanishes for increasing decay rates. The same characteristics with the overshoot are also seen in the scenario with a linear parameterization of K_z. Here the air-clearance time was approximately 2-3 orders of magnitude smaller than for the scenarios with constant K_z. We also showed an example of how to implement a more realistic time-dependent resuspension-rate, describing the aspects of countermeasures for a biological incident. The model also allows for investigating other scenarios, for example, wet deposition of the contaminant due to rainout and washout, and for estimating the air-clearance time due to resuspension of material caused by movement in a surface contaminated area. Future work will focus on additional transport and removal mechanisms, including activity-dependent resuspension in a hybrid model with continuous dispersion in air coupled with agent-based activity on the surface. The air-surface exchange formulation presented here may also be incorporated into higher-dimensional atmospheric dispersion frameworks to investigate the interaction between transport, deposition, resuspension, and surface inactivation in more complex environments.

Code and data availability. The VADERS model source code is available under the MIT License at https://github.com/MskytteP/VADERS. The exact version used to generate the results presented in this paper is archived on Zenodo at: https://doi.org/10.5281/zenodo.22790822, Liboriussen (2026). The archive contains the model source code, numerical verification scripts, figure-generation scripts, and the data required to reproduce the simulations presented in this study.

Appendix A: Derivations of reference cases

A detailed derivation of the solution to the reference cases (ii) is shown here. The derivation of case (i) follows the same approach and is therefore omitted. From Eq. (9) we have

$$\frac{\partial a}{\partial t} = \frac{1}{Pe}\frac{\partial^2 a}{\partial z^2} + \frac{\partial a}{\partial z}. \tag{A1}$$

Assuming a separable solution we can write a as

$$a(z,t) = v(z,t)\,\phi(z,t), \tag{A2}$$

where $\phi(z,t) = e^{\gamma z + \epsilon t}$ and inserting in Eq. (A1), we get

$$\frac{\partial v}{\partial t} + \left(\epsilon - \gamma - \frac{\gamma^2}{Pe}\right) v - \left(1 + \frac{2\gamma}{Pe}\right)\frac{\partial v}{\partial z} = \frac{\partial^2 v}{\partial z^2}. \tag{A3}$$

If $\epsilon = -\frac{Pe}{4}$ and $\gamma = -\frac{Pe}{2}$, then Eq. (A3) has the form of a pure diffusion equation which can be solved using separation of variables

$$\frac{\partial v}{\partial t} = \frac{1}{Pe}\frac{\partial^2 v}{\partial z^2}. \tag{A4}$$

https://doi.org/10.5194/egusphere-2026-5623
Preprint. Discussion started: 12 November 2026
© Author(s) 2026. CC BY 4.0 License.

The boundary conditions for the transformed variable is,

$$\frac{\partial v(0,t)}{\partial z} + \frac{Pe}{2} v(0,t) = 0 \tag{A5}$$

$$v(1,t) = 0\,. \tag{A6}$$

By separation of variables, $v(z,t) = Z(z)T(t)$, we get from Eq. (A4)

$$Z'' = -\lambda Z \tag{A7}$$

$$T' = -\frac{1}{Pe}\lambda T, \tag{A8}$$

which by the assumption of $Z(z) = e^{rz}$ Eq. (A7) gives

$$r = \pm\sqrt{-\lambda}. \tag{A9}$$

λ is a separation constant that will be determined in the following subsections. Note that by separation of variables we get the following boundary conditions for Z from Eqs. (A5) and (A6)

$$\frac{\partial Z(0)}{\partial z} + \frac{Pe}{2} Z(0) = 0 \tag{A10}$$

$$Z(1) = 0\,. \tag{A11}$$

Eqs. (A7), (A10) and (A11) is a regular Sturm-Liouville problem, and we will use the properties from this later on.

A1 Case 1: $\lambda = \kappa^2 > 0$

The general solution is

$$Z\left(z\right) = C_1 \cos\left(\kappa z\right) + C_2 \sin\left(\kappa z\right). \tag{A12}$$

By inserting Eq. (A12), in Eqs. (A10) and (A11) we get

$$C_2\kappa + \frac{Pe}{2} C_1 = 0 \tag{A13}$$

$$C_1 \cos\left(\kappa\right) + C_2 \sin\left(\kappa\right) = 0, \tag{A14}$$

which has non-trivial solutions when

$$\tan(k) = \frac{2\kappa}{Pe}. \tag{A15}$$

Let $C_1 = 1$ then from Eq. (A13) we have $C_2 = -\frac{Pe}{2\kappa}$, which implies

$$Z(z) = \cos\left(\kappa z\right) - \frac{Pe}{2\kappa} \sin\left(\kappa z\right). \tag{A16}$$

https://doi.org/10.5194/egusphere-2026-5623
Preprint. Discussion started: 12 November 2026
© Author(s) 2026. CC BY 4.0 License.

Using the solutions to Eqs. (A7) and (A8) we can write the seperated solution as

$$Z_n(z)T_n(t) = \left(\cos(\kappa_n z) - \frac{Pe}{2\kappa_n}\sin(\kappa_n z)\right) C_3 e^{-\frac{\kappa_n^2}{Pe}t}, \tag{A17}$$

where Z_n is the spatial eigenfunctions. The values for κ_n can be found be solving Eq. (A15) for the values of κ with the Newton-Raphson method, Epperson (2013). The eigenfunction expansion where A_n satisfies the initial conditions is given by

$$v(z,t) = \sum_{n=1}^{\infty} A_n \left(\cos(\kappa_n z) - \frac{Pe}{2\kappa_n}\sin(\kappa_n z)\right) e^{-\frac{\kappa_n^2}{Pe}t}. \tag{A18}$$

The values of A_n can be found by writing the equation for the transformed variable, a, at $t = 0$ with a given initial condition $f_0(z)$

$$a(z,0) = v(z,0)e^{-\frac{Pe}{2}z} = f_0(z) \tag{A19}$$

$$\Rightarrow v(z,0) = e^{\frac{Pe}{2}z} f_0(z) \quad . \tag{A20}$$

Multiplying Eq. (A20) by Z_m, integrating from 0 to 1 on both sides and moving $\sum_{n=1}^{\infty} A_n$ outside the integral we have

$$\sum_{n=1}^{\infty} A_n \langle Z_n, Z_m \rangle = \left\langle Z_m e^{\frac{Pe}{2}z}, f_0 \right\rangle, \tag{A21}$$

where the inner product is defined as

$$\langle g, h \rangle = \int_0^1 g(z)h(z)dz. \tag{A22}$$

We can use the property of orthogonality of the eigenfunctions to simplify Eq. (A21)

$$A_m \langle Z_m, Z_m \rangle = \left\langle Z_m e^{\frac{Pe}{2}z}, f_0 \right\rangle$$

$$\Rightarrow A_n = \frac{\left\langle Z_n e^{\frac{Pe}{2}z}, f_0 \right\rangle}{||Z_n||^2} \tag{A23}$$

With an expression for A_n and $v(z,t)$, see Eqs. (A23) and (A18) respectively, and by Eq. (A2) the solution to the initial-boundary-value-problem is

$$a(z,t) = \phi(z,t) \sum_{n=1}^{\infty} A_n \left(\cos(\kappa_n z) - \frac{Pe}{2\kappa_n}\sin(\kappa_n z)\right) e^{-\frac{\kappa_n^2}{Pe}t}. \tag{A24}$$

This solution holds for $Pe < 2$. When $Pe \geq 2$ the solution contains additional eigenvalue modes, a hyperbolic mode for $Pe > 2$ and a zero mode for $Pe = 2$, which is shown here.

A2 Case 2: $\lambda = 0$

In this case the general solutions to Eqs. (A7) and (A8) is

$$Z(z) = az + b \tag{A25}$$

$$T(t) = c. \tag{A26}$$

https://doi.org/10.5194/egusphere-2026-5623
Preprint. Discussion started: 12 November 2026
© Author(s) 2026. CC BY 4.0 License.

From the boundary conditions, see Eqs. (A10) and (A11) we get

$$a = -b \tag{A27}$$

$$\Rightarrow b\left(\frac{Pe}{2} - 1\right) = 0, \tag{A28}$$

which is satisfied when in the case where $Pe = 2$. This implies an additional zero eigenvalue mode when $Pe = 2$ to the modes from Case 1. Let $b = 1$ and $c = 1$ we have the zero mode solution as

$$v_0(z,t) = A_0 Z_0 = A_0(1 - z), \tag{A29}$$

where A_0 is determined by the initial conditions as in Eq. (A23). If we let $Pe = 2$ and $\kappa_n \to 0$ and sum from 0 to ∞, we will get the zero mode expressed in Eq. (A18). So the final solution has the same general form as for case 1 when $Pe = 2$, with eigenvalues $\lambda_n \geq 0$.

A3 Case 3: $\lambda = -\kappa^2 < 0$

For case 3 we can write the distinct roots from Eq. (A9) as

$$r = \pm\kappa \tag{A30}$$

which gives a general solution for the spatial variable as

$$Z(z) = C_1 e^{\kappa z} + C_2 e^{-\kappa z}. \tag{A31}$$

By inserting the boundary conditions from Eqs. (A5) and (A6) we get the relation

$$\frac{\kappa + \frac{Pe}{2}}{\frac{Pe}{2} - 1} = e^{2\kappa}, \tag{A32}$$

which is satisfied when $Pe > 2$. By rewriting the general solution for Z as

$$Z(z) = C_1 \cosh(\kappa z) + C_2 \sinh(\kappa z), \tag{A33}$$

we obtain the non-trivial solutions for the boundary conditions as

$$\tanh(k) = \frac{2\kappa}{Pe}, \tag{A34}$$

which can also be solved by the Newton-Raphson method. For $Pe > 2$ Eq. (A34) only has one positive distinct root which implies an additional eigenmode to the final solution in case 1, see Eq. (A24). Combining the three cases we can write the final solution to the initial-boundary-value-problem as

$$a(z,t) = \phi(z,t)\left(Y_0(z,t) - Y_1(z,t)\right) \tag{A35}$$

https://doi.org/10.5194/egusphere-2026-5623
Preprint. Discussion started: 12 November 2026
© Author(s) 2026. CC BY 4.0 License.

where

$$Y_0 = \chi_0(z,t) + \sum_{n=1}^{\infty} A_n \cos(\kappa_n z)\, e^{-\frac{\kappa_n^2}{Pe}t}, \tag{A36}$$

and

$$Y_1 = \chi_1(z,t) + \frac{Pe}{2}\sum_{n=1}^{\infty} \frac{A_n}{\kappa_n} \sin(\kappa_n z)\, e^{-\frac{\kappa_n^2}{Pe}t}. \tag{A37}$$

$\chi_1(z,t)$ and $\chi_2(z,t)$ is given by

$$\chi_0(z,t) = \begin{cases} 0, & \text{if } Pe < 2 \\ A_0, & \text{if } Pe = 2 \\ A_{\kappa_0} \cosh(\kappa_0 z)\, e^{\frac{\kappa_0^2}{Pe}t}, & \text{if } Pe > 2, \end{cases} \tag{A38}$$

and

$$\chi_1(z,t) = \begin{cases} 0, & \text{if } Pe < 2 \\ A_0 z, & \text{if } Pe = 2 \\ \frac{Pe}{2}\frac{A_{\kappa_0}}{\kappa_0} \sinh(\kappa_0 z)\, e^{\frac{\kappa_0^2}{Pe}t}, & \text{if } Pe > 2\,. \end{cases} \tag{A39}$$

A_0 and A_{κ_0} is found by the same method as in Eqs. (A20) - (A23) with the expression for v and Z given by the cases, see Eq. (A29) for case 2 and Eq. (A33) with $C_1 = 1$ and $C_2 = -\frac{Pe}{2k}$ for case 3.

A4 Estimating relaxation time for large Pe

For the additional eigenmode given by Eq. (A34) we can approximate κ for large Pe by using the exponential definition of tanh

$$\tanh(\kappa) = \frac{1 - e^{-2\kappa}}{1 + e^{-2\kappa}}\,. \tag{A40}$$

For large Pe we have large κ, which implies that $e^{-2\kappa} \ll 1$. Rewriting Eq. (A40) and expanding the denominator as geometric series

$$\tanh(\kappa) = \frac{1-\epsilon}{1+\epsilon} = (1-\epsilon)(1-\epsilon+\epsilon^2-...) \tag{A41}$$

$$= 1 - 2\epsilon + 2\epsilon^2 - ....\tag{A42}$$

Substituting $e^{-2\kappa}$ back in Eq. (A42) we observe that $e^{-2\kappa} \ll e^{-4\kappa}$ for large κ. We approximate Eq. (A34) as

$$1 - 2e^{-2\kappa} \approx \frac{2\kappa}{Pe}\,. \tag{A43}$$

By rewriting Eq. (A43) as

$$\frac{Pe}{2} - \kappa \approx Pe e^{-2\kappa}, \tag{A44}$$

https://doi.org/10.5194/egusphere-2026-5623
Preprint. Discussion started: 12 November 2026
© Author(s) 2026. CC BY 4.0 License.

and define the small difference

$$\delta = \frac{Pe}{2} - \kappa, \tag{A45}$$

we have

$$\delta \approx Pee^{-2(\frac{Pe}{2}-\delta)} = Pee^{-Pe}e^{2\delta}. \tag{A46}$$

Since δ is small, we have $e^{2\delta} \approx 1$. Rearranging Eq. (A45) and insert in the expression for the relaxation time for the additional wave vector we have

$$t_0 = \frac{Pe}{\frac{Pe}{4} - \kappa^2} \tag{A47}$$

$$\Rightarrow t_0 = \frac{Pe}{\frac{Pe}{4} - \frac{Pe}{4} + Pe\delta - \delta^2}. \tag{A48}$$

Since $\delta^2 \ll Pe\delta$ we can ignore the last term in the denominator. Using this and inserting the relation from Eq. (A46), we can express the dependency of t_0 on Pe as

$$t_0 \approx \frac{1}{\delta} \approx \frac{1}{Pe}e^{Pe}. \tag{A49}$$

Appendix B: Numerical Methods

We used a one-dimensional finite-volume method with first-order upwind advection and explicit Euler time integration to solve the model in the scenarios used to investigate the lower flux exchange boundary condition. The solver was first evaluated by assessing mass conservation of the airborne and surface concentrations in a closed system with an upper homogeneous Robin boundary condition. This verification was done with $Pe = 4$ and $\Lambda^*_{\text{res}}/v^*_{\text{dep}} = 0.1$, and no significant changes in the mass was observed, see Fig. B1.

The numerical solution was verified against the analytical solutions for cases (i) and (ii) described in the paper. Figs. B2 and B3 show the relative L_2 error, defined as

$$E_{L_2} = \frac{\|a_{\text{num}} - a_{\text{ana}}\|_2}{\|a_{\text{ana}}\|_2}, \tag{B1}$$

, where a_{num} and a_{ana} is the numerical and analytical concentrations, respectively. The discrete L_2 norm is evaluated as

$$\|a\|_2 = \left(\sum_{i=1}^{N} a_i^2 \, \Delta z\right)^{1/2}, \tag{B2}$$

which corresponds to a finite-volume approximation of the continuous L_2 norm. The verification was performed for $Pe = 0.3, 1$ and 4, and N $= 250, 500$ and 1000, where N is the number of cells. As expected the relativeL_2 error decreases with increasing grid resolution for the different Pe-cases, demonstrating convergence of the numerical solution towards the analytical solution. Unless otherwise stated, all the reported results the FV-solver was set up with 250 cells and we chose the size of the time-steps so the stability-conditions was satisfied.

https://doi.org/10.5194/egusphere-2026-5623
Preprint. Discussion started: 12 November 2026
© Author(s) 2026. CC BY 4.0 License.

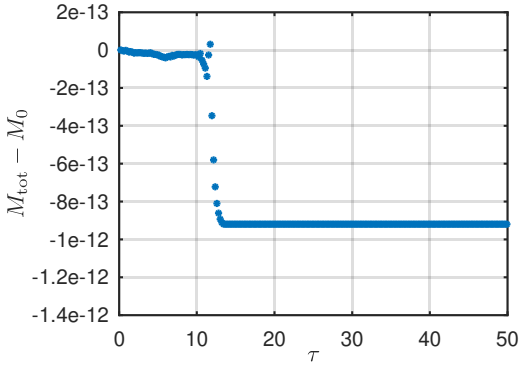


Figure B1. $M_{\text{tot}} - M_0$, where M_{tot} is the total mass in the system defined by $M_{\text{tot}} = M_{\text{air}} + M_{\text{surface}}$ and M_0 is the initial mass of the system. The parameter settings for this verification was $\Lambda^*_{\text{res}}/v^*_{\text{dep}} = 0.1$ and $Pe = 4$.

https://doi.org/10.5194/egusphere-2026-5623
Preprint. Discussion started: 12 November 2026
© Author(s) 2026. CC BY 4.0 License.

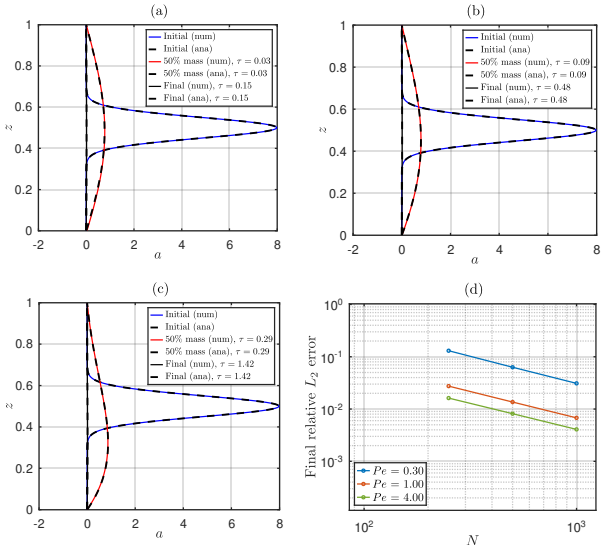


Figure B2. (a)-(c) Numerical (solid lines) and analytical (dashed lines) concentration profiles for case (i) at three stages of the simulation: the initial condition, 50 % of the airborne mass remaining, and 1 % of the airborne mass remaining. Panels (a), (b), and (c) correspond to $Pe = 0.3$, $Pe = 1$, and $Pe = 4$, respectively, using $N = 250$ grid cells. (d) Relative L_2 error at the final simulation stage (1 % airborne mass remaining) as a function of grid resolution.

https://doi.org/10.5194/egusphere-2026-5623
Preprint. Discussion started: 12 November 2026
© Author(s) 2026. CC BY 4.0 License.

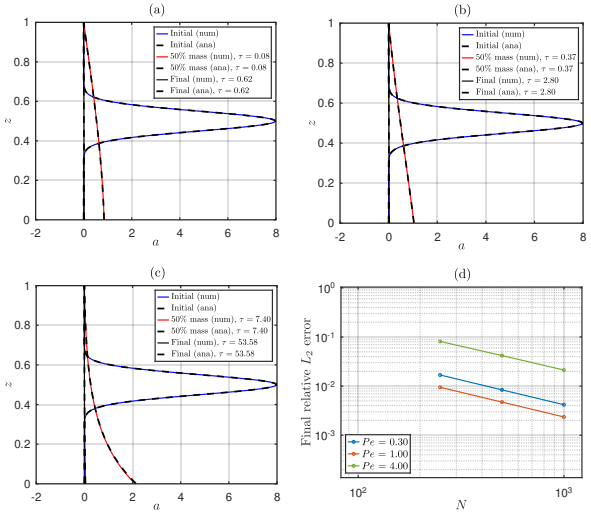


Figure B3. (a)-(c) Numerical (solid lines) and analytical (dashed lines) concentration profiles for case (ii) at three stages of the simulation: the initial condition, 50 % of the airborne mass remaining, and 1 % of the airborne mass remaining. Panels (a), (b), and (c) correspond to $Pe = 0.3$, $Pe = 1$, and $Pe = 4$, respectively, using $N = 250$ grid cells. (d) Relative L_2 error at the final simulation stage (1 % airborne mass remaining) as a function of grid resolution.

https://doi.org/10.5194/egusphere-2026-5623
Preprint. Discussion started: 12 November 2026
© Author(s) 2026. CC BY 4.0 License.

Author contributions. MSL and JSH conceptualized the model. MSL implemented the numerical code, performed the simulations and analysis, and prepared the figures. MSL wrote the original manuscript draft. JSH supervised the work, contributed to the scientific interpretation, and reviewed and edited the manuscript.

Competing interests. The authors declare that they have no conflict of interest.

Acknowledgements. The authors would like to thank Vibeke Østergaard Thomsen for valuable discussions about emergency response following a biological incident and for comments on the general structure of the paper. The authors used Microsoft Copilot as a language and coding assistance tool for improving the clarity and readability of parts of the manuscript. All scientific content, model development, analysis, interpretation of results, and final manuscript revisions were performed and verified by the authors.

https://doi.org/10.5194/egusphere-2026-5623
Preprint. Discussion started: 12 November 2026
© Author(s) 2026. CC BY 4.0 License.

References

Calder, K. L.: ATMOSPHERIC DIFFUSION OF PARTICULATE MATERIAL, CONSIDERED AS A BOUNDARY VALUE PROBLEM, Journal of Atmospheric Sciences, 18, 413–415, https://doi.org/10.1175/1520-0469(1961)018<0413:ADOPMC>2.0.CO;2, 1961.

Epperson, J. F.: An Introduction to Numerical Methods and Analysis, Wiley, Hoboken, 2 edn., ISBN 9781118730973, 2013.

Farlow, S. J.: Partial Differential Equations for Scientists and Engineers, Dover Publications, Inc., New York, ISBN 0-486-67620-X, 1993.

Franco, C. and Bouri, N.: Environmental decontamination following a large-scale bioterrorism attack: federal progress and remaining gaps, Biosecurity and bioterrorism : biodefense strategy, practice, and science, 8, 107–17, https://doi.org/10.1089/bsp.2010.0009, 2010.

Giardina, M. and Buffa, P.: A new approach for modeling dry deposition velocity of particles, Atmospheric Environment, 180, 11–22, https://doi.org/10.1016/j.atmosenv.2018.02.038, 2018.

Glinowiecka-Cox, M. B.: Analytic Solution of 1D Diffusion-Convection Equation with Varying Boundary Conditions, University Honors Theses, https://doi.org/10.15760/honors.1224, 2022.

Henry, C., Minier, J.-P., and Brambilla, S.: Particle resuspension: Challenges and perspectives for future models, Physics Reports, 1007, 1–98, https://doi.org/10.1016/j.physrep.2022.12.005, 2023.

Layshock, J. A., Pearson, B., Crockett, K., Brown, M. J., Cuyk, S. V., Daniel, W. B., and Omberg, K. M.: Reaerosolization of Bacillus spp. in Outdoor Environments: A Review of the Experimental Literature, Biosecurity and Bioterrorism: Biodefense Strategy, Practice, and Science, 10, 299–303, https://doi.org/10.1089/bsp.2012.0026, 2012.

Liboriussen, M. S.: VADERS v1.0.0, https://doi.org/10.5281/zenodo.22790822, 2026.

Monin, A. S. and Obukhov, A. M.: Basic laws of turbulent mixing in the surface layer of the atmosphere, Tr. Akad. Nauk SSSR Geophiz. Inst., 24, 163–187, https://www2.mmm.ucar.edu/wrf/users/physics/phys_references.html#SL, english translation by J. Miller, Translation No. 1234, 1959; electronic version prepared by K. McNaughton, 2008, 1954.

Nicholson, K.: A review of particle resuspension, Atmospheric Environment (1967), 22, 2639–2651, https://doi.org/10.1016/0004-6981(88)90433-7, 1988.

Richardson, L. F.: Atmospheric diffusion shown on a distance-neighbour graph, Proceedings of the Royal Society of London. Series A, Containing Papers of a Mathematical and Physical Character, 110, 709–737, https://doi.org/10.1098/rspa.1926.0043, 1926.

Salem, H. and Katz, S. A.: Aerobiology: The Toxicology of Airborne Pathogens and Toxins, The Royal Society of Chemistry, ISBN 978-1-84973-594-0, https://doi.org/10.1039/9781849737913, 2016.

Sehmel, G.: Particle resuspension: A review, Environment International, 4, 107–127, https://doi.org/10.1016/0160-4120(80)90005-7, 1980a.

Sehmel, G. A.: Particle and gas dry deposition: A review, Atmospheric Environment (1967), 14, 983–1011, https://doi.org/10.1016/0004-6981(80)90031-1, 1980b.

Slinn, W.: Formulation and a solution of the diffusion-deposition-resuspension problem, Atmospheric Environment (1967), 10, 763–768, https://doi.org/10.1016/0004-6981(76)90077-9, 1976.

Stull, R. B.: An Introduction to Boundary Layer Meteorology, Springer Dordrecht, https://doi.org/10.1007/978-94-009-3027-8, 1988.

Sutton, O. G.: Micrometeorology, McGraw–Hill, New York, 1953.

Taylor, G. I.: Diffusion by Continuous Movements, Proceedings of the London Mathematical Society, s2-20, 196–212, https://doi.org/10.1112/plms/s2-20.1.196, 1922.